Journal of Machine Engineering, 2024, Vol. 24
ISSN 1895-7595 (Print) ISSN 2391-8071 (Online)

Received*: 11 July 2024* / Accepted: *18 November 2024* / Published online: *26 November 2024*

machine tool, CFD simulation,
thermal error, tool cooling

Christian NAUMANN[1*], Claus-Dieter SCHMIDT[1],
Alexander GEIST[1], Steffen BRIER[2],
Janine GLÄNZEL[1], Philipp KLIMANT[1,4]
Steffen IHLENFELDT[1,3], Martin DIX[1,2].

INVESTIGATION OF TOOL COOLING AND HEAT TRANSFER USING COMPUTATIONAL FLUID DYNAMICS SIMULATIONS

Thermal errors remain one of the biggest challenges for the precision of cutting machine tools. Aside from optimizations in the machine tool design and behaviour, optimal cutting process parameters and targeted usage of cutting fluid or alternative methods of tool cooling are required for improved process efficiency with minimal energy demand and maximal tool life. A simulation-based study is presented which compares both different methods of tool cooling, specifically air cooling, flooded cooling and minimum quantity lubrication and also different simulation methods and models. Using a case study, which models an existing thermal test stand comprised of motor spindle, tool holder, tool and coolant nozzle, different cooling scenarios were tested and compared. The simulations were performed in ANSYS CFX. Comparisons were made between simulations with and without buoyancy, with and without tool rotation, transient and steady-state, with laminar flow and with different turbulence models and between the different cooling scenarios. Some insight on different time step sizes and the resulting increase in simulation time and precision was also gained. These results will make future studies on the thermal behaviour of both tool and cutting process easier by showing suitable simulation techniques and viable model simplifications.

1. INTRODUCTION

In machine tool operations, thermal errors are most often predominant over geometric, static and dynamically induced errors [1]. Therefore, energy-intensive cooling systems are commonly used to reduce thermally induced structural deformations in machine tools. Coolant has several functions during the machining process [2]. Its primary functions are to cool the cutting area and to reduce friction through added lubricant. During the machining process, the cutting fluid serves the purpose of reducing the temperature of the tool and the

[1] Fraunhofer Institute for Machine Tools and Forming Technology IWU Chemnitz, Germany,
[2] Institute for Machine Tools and Production Processes, Chemnitz University of Technology, Germany,
[3] Machine Tool Development and Adaptive Controls, Technical University Dresden, Germany,
[4] Virtual Technologies, University of Applied Sciences Mittweida, Germany,
[*] E-mail: christian.naumann@iwu.fraunhofer.de
https://doi.org/10.36897/jme/196074

workpiece, as well as minimizing wear on the tool. However, it is important to note that the cooling lubricant is distributed throughout the entire workspace of the machine tool, thereby cooling (or in some cases warming) all of its components [3]. Mayr et al. found that the use of coolant significantly affects TCP displacement by comparing machine behaviour during coolant usage and in dry conditions [4]. In their investigation, the use of cutting fluid even showed increased temperatures and thermal errors, especially in the machining table, due to the coolant usage, which in this case was not cooled before recirculation. Pavlicek et al. (2016) conducted a comparison between the usage of standard cooling lubricant and CO2 cooling in a machine tool. The results showed that the usage of CO2 reduced the thermo-elastic deformation of one of the axes by more than 60% [5]. Hernandez-Becerro et al. (2017) investigated the influence of the supply of cutting fluid in the workspace on the thermo-elastic deformation [6]. The investigated machine tool had three separate cutting fluid supply systems for spindle head, machine bed and workspace shower. The study found that some supply systems affect certain thermal error components, while others remain unaffected. The *y*-inclination was, e.g., largely unaffected by cutting fluid, while the *z*-inclination was strongly affected and was minimal with the spindle head supply used by itself without the other two supply systems.

Studies performed by Bräunig et al. (2015) and Perri et al. (2016) have investigated the effects of air cooling on the tool deformation [7, 8]. The results indicate that pressured air cooling can reduce the temperature increase in the tool by up to 50% compared to dry machining without any cooling. In addition to providing a better cooling effect, the use of cooling lubricant also significantly affects air quality. Depending on the main spindle speed, a significant concentration of fog particles may be released into the environment, which can pose health risks under regular exposure [9].

An early work by Daniel et al. (1996) focused on calculating the heat transfer at the workpiece, which is essential for understanding thermal workpiece behaviour [10]. This calculation was previously determined for turning in a one-dimensional view using different oils. It is known that the emulsion coolant used in high-speed milling with minimum quantity lubrication (MQL) is inefficient because it cannot reach the inner zones of the tool teeth. The coolant flow has three distinct effects in the cutting zone: it acts on the tool, on the workpiece, and it also removes chips. To achieve optimal cooling, the nozzle position relative to the feed direction is crucial, as Lopez et al. (2006) have shown [11]. It may therefore be beneficial to arrange multiple nozzles that can be activated or deactivated depending on the feed direction.

Brecher et al. (2012) analysed and compared different decentral cooling systems with regard to their power consumption for a sample machining centre [12]. To achieve this, the power consumption of this machining centre was analysed for different operating conditions. Besides power, displacement of the TCP and further variables such as pressure, flow rate and temperature were monitored for the different machining conditions and cooling systems. The impact of these scenarios on the machine structure remains largely unknown. Therefore, a metrological and numerical investigation was conducted by Bräunig et al. (2018) to identify the thermal behavior of a machine tool workspace under different cooling scenarios [13].

Dehn et al. (2023) investigated the effects of tool cooling on the thermal error and presented a method on how to measure the thermo-elastic machine behaviour using integrated deformation sensors to compute the TCP displacement during coolant usage [14]. Similarly,

Kizaki et al. (2021) have developed a robust thermal error prediction method using a novel temperature measurement system called LATSIS, which uses 284 temperature sensors covering almost the entire machine tool, to reconstruct the 3D temperature field and with it estimate the thermal error [3]. It allowed very accurate thermal error predictions even under large thermal disturbances from cutting fluid use.

Jedrzejewski et al. have demonstrated the importance of a holistic cooling system design to optimize cooling effects (and thus thermal error) with minimal energy consumption [15]. They have concluded that one very important aspect of this is knowing (by measuring or accurately predicting) the power losses of all relevant heat sources and designing the cooling systems both in strength and location accordingly.

A new FEM modelling technique by Tanabe et al. uses two types of virtual elements to better include convection effects in the workspace into the thermal FEM simulation [16]. The resulting model showed a good agreement with the corresponding experiment, though it is limited in assuming a steady laminar air flow in the workspace.

Mareš et al. have investigated the effects of cutting fluid temperature on the machine tool thermal error and tested different methods of fluid temperature control [17]. They were able to show that fixed fluid temperature regulation reduced thermal displacements compared to non-cooled machining and that gradient regulation achieved an additional improvement of two orders of magnitude. Fix, in this case, refers to regulating the heat exchanger for the cutting fluid to achieve constant output temperature, whereas in gradient regulation the output is variable depending on temperature readings from the machine structure.

One major practical problem with computational fluid dynamics (CFD) simulations is that they take a long time to compute, even for relatively simple stationary load scenarios. Kumar et al. have presented an effective method for reducing computation times for CFD simulations using a novel parallel computing approach [18]. By running not only the different load cases but each individual load case in parallel, they were able to achieve a 31-fold speed-up on a high-performance computing cluster.

The previous works of many research groups have independently investigated and shown the large effects of cutting fluid and various similar tool cooling systems on the thermal behaviour of both cutting tool and workspace. However, the effects of cutting fluid on the thermal behaviour of the machine tool as a whole is still not fully understood, as much of it depends on variable process and operational parameters. Since experimental investigations are costly and time-consuming and they always only illuminate very specific experimental conditions, simulation-based studies, where different system parameters can easily be changed and tested, are the most suitable path to obtaining more generalized information on the thermal interaction between coolant, tool and machine. Nevertheless, experimental validation remains important to ensure confidence in the computed scenarios.

This paper aims to investigate the thermal influence of dry cutting, air cooling and flood cooling on the tool and workspace, and particularly on how to model these effects in CFD simulations. Chapter 2 describes the model, which is a close representation of an experimental setup. Chapter 3 highlights simulation results under different cooling scenarios and simulation settings. Chapter 4 shows some experimental results, which partially contradict some of the simulation results under flood cooling with fast tool rotation. It also gives a theory on the differences between the previous simulation results and the measurements and shows how an

improved simulation model can obtain more realistic results. A brief analysis of the resulting thermal deformation is also given to show the relevance of correct cooling modelling. Chapter 5 briefly elaborates on the role of chips in tool cooling, which was mostly neglected in the present study. The paper concludes with a short summary and outlook on future research.

2. DESCRIPTION OF THE SIMULATION MODEL AND SCENARIOS

One of the largest uncertainties in simulating the thermal state of a machine tool during machining operations is still the cutting process and everything associated with it within the machine tool workspace. This especially includes the cutting fluid, the chips, the tool, the workpiece and the air within the workspace. In order to better model the whole process, it is best to start with the individual contributing part. Therefore, in this study the focus was placed on the heating and cooling of the tool under different cooling strategies (e.g. air and flooded cooling) and the different methods for simulating these effects. For this, the machine tool itself is irrelevant, only the fact that it is a horizontal machining centre. Rather than studying the entire machine, a simpler test stand was constructed, which comprises only the motor spindle, the tool holder, the tool and cooling nozzles, which can deliver cutting fluid and compressed air, respectively. The corresponding simulation model also contains a workpiece with a clamping device, though this will not be needed here and is for future studies only. Figure 1 shows the setup with the entire modelled air volume on the left and a magnified view of the cutting zone on the right. The workspace has dimensions of 526 mm × 1294 mm × 1698 mm. There is a cylindrical outlet for the evacuation unit positioned at the top of the workspace. The entire bottom face not covered by the table is modelled as an opening, which permits air to enter and leave freely, depending on the current air pressure in the workspace. It also allows the cutting fluid to flow out of the workspace. This was done because the bottom of machine tools usually has such openings for removal of chips and cutting fluid.

The original CAD model was simplified / modified by removing bore holes, changing the tool holder geometry to better match the real test stand, including air outlets at the top and bottom of the workspace, adding a cuboid-shaped housing and adding the coolant nozzle in the appropriate location. Triangulation (meshing) was done using the Siemens NX software. The final mesh comprised 3,090,138 tetrahedral elements and 618,780 nodes. Since the main focus was the tool and its adjacent areas, a cylindrical hull was placed around it to get a more accurate result for this region, see Fig. 2, right. This extra fluid domain allows the simulation of rotating fluids while keeping the bulk of the workspace stationary.

Table 1 lists the various elements comprising the simulation model and their corresponding mesh sizes and materials. The coolant nozzle was given a volume flow rate of 1.25 l/min corresponding to a flow velocity of around 0.74 m/s. The initial temperature for the cutting fluid as it leaves the nozzle was 22°C. Figure 2 (left) shows the positioning of the nozzle relative to the tool and spindle. It is “aimed” at the very front of the tool where the cutting occurs and the corresponding heat is introduced into tool and workpiece. For the outlets, standard atmospheric pressure (1013.25 hPa) was used. The temperature of the workspace wall was set to a constant 20°C. For the transient simulations, the starting temperature for the solid objects in the workspace was also set to 20°C. The boundary

conditions of the wall in the CFD simulation model are “no slip” with a fixed temperature of 20°C and no wall adhesion.

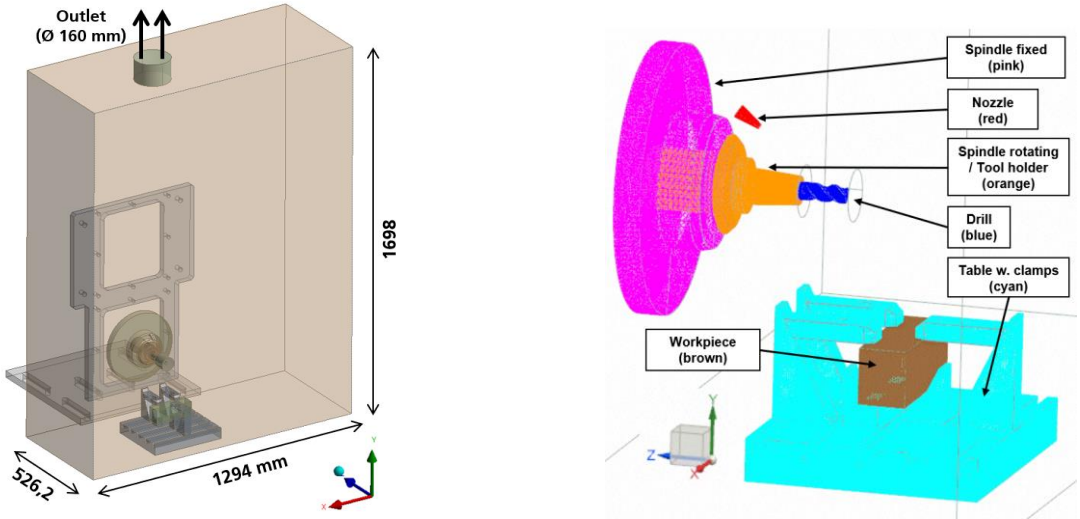

Fig. 1. CAD model of milling test stand

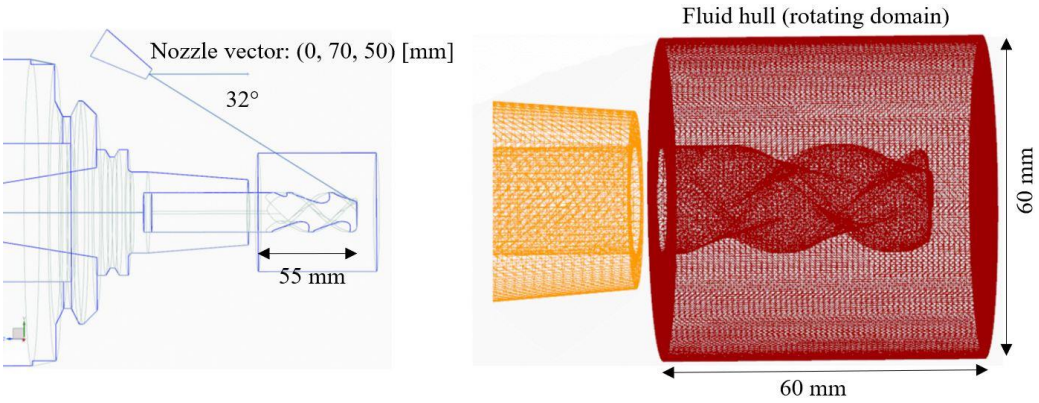

Fig. 2. Left: coolant nozzle positioning; Right: CFD model surrounding the tool

Table 1. Test stand components and mesh sizes

Assembly	N° elements	N° vertices	Material
Workspace	1,486,823	292,599	Air
Tool hull	470,767	89,696	Air
Tool (straight shank drill bit)	66,767	14,970	Steel
Spindle (rotating part)	94,455	20,556	Steel
Spindle (stationary part)	57,177	13,039	Steel
Coolant nozzle	2,432	669	Steel
Workpiece	97,659	19,725	Aluminium
Workpiece holder and clamps	814,058	167,526	Steel

The heat from the simulated process was introduced from the front surface of the tool. The heat flux was set to 99 kW/m², which, for the given surface area, is approximately 12.7 W. This specific heat flux was chosen because it is the maximum that the induction heater can

supply consistently in the real test stand. Ignoring coolant, spindle and tool rotation and buoyancy, this constant heat flux would heat the front of the tool to 100.1°C. The average temperature of the helical tool section was 60.6°C. Figure 3 shows the temperature field of tool and spindle for this stationary state.

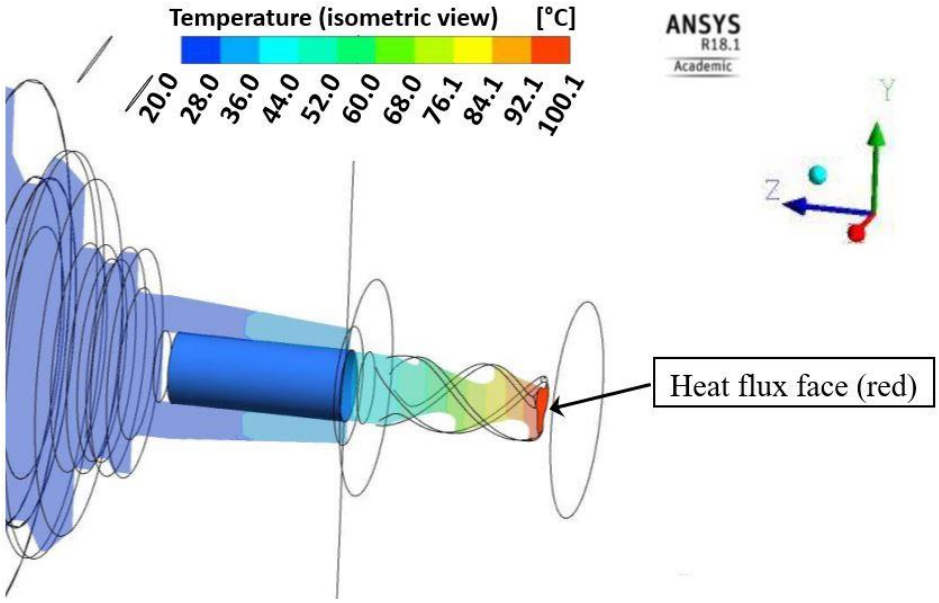

Fig. 3. Temperature field in stationary state with heat influx from tool front

Four load cases with different cooling scenarios were simulated:

- load case 1: cooling with pure water,
- load case 2: cooling with 94% water and 6% lubricant,
- load case 3: cooling with compressed air,
- load case 4: cooling with 94% compressed air and 6% lubricant.

3. SIMULATION RESULTS FOR DIFFERENT COOLING SCENARIOS AND SIMULATION SETTINGS

3.1. TEST OF SOLVER PARAMETERS

Calculating the solution for both the stationary and transient load cases in ANSYS CFX was more difficult than expected. For the transient simulation without tool rotation, very short time steps of 0.1s were needed to obtain a stable solution. This, in turn, led to long computation times, e.g., a five-minute time frame took two days and four hours using four cores. For the stationary simulation, the auto-timescale factor of one led to successful results. 2,000 numerical iterations on three cores took around one day and 17 hours. Later tests showed that 500 iterations were already sufficient to obtain accurate results. The limitation to three cores was due to the software crashing occasionally after a few hours in the original

(older) ANSYS version. In the current version (2023 R2), no problems with higher core numbers were detected, yet.

It was generally the case, that stationary simulations took less time to compute than transient ones. For the transient simulations with tool rotation (3,000 rpm), a time step size of 0.01 s worked well. This roughly corresponds to two time steps per revolution. With eight cores, the five-minute time frame was computed in 13 days and 21 hours. Increasing the time step to 0.1s led to a large variance in the simulation results. A refinement to 0.0025 s time steps led to a further reduction in the variance of both average and maximum drill temperatures. However, this also increased the computation time for five minutes to 54 days and 23 hours with eight cores. Clearly, such computation times are unacceptably high for all practical purposes. Figure 4 shows the influence of different time step sizes on the average and maximum tool temperatures for the same load case.

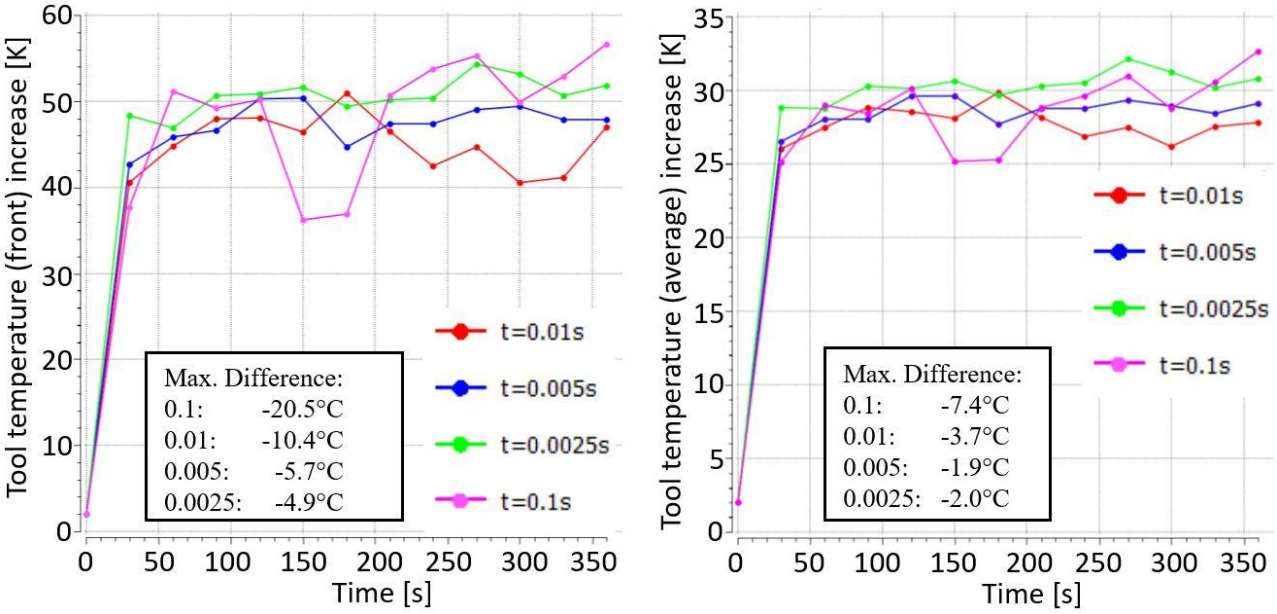

Fig. 4. Transient tool max. (left) and mean (right) temperatures for different simulation time step sizes

Looking only at the final temperatures, towards which the temperature curves converge, there is no clear trend visible, which correlates to the decreasing time step sizes from 0.1 s (pink) to 0.0025 s (green). There is, however, a clear trend towards decreasing temperature variations for decreasing time steps after the first minute of simulated time. Table 2 compares the computation time for all four simulation runs with eight cores, which was the maximum available core number.

In CFD simulations, the results generally become reliable after the convergence residuals of state quantities drop under a certain level. Convergence was verified on all simulations. In the workspace, ANSYS can, e.g., display the momentum and mass charts for fluid regions or the heat transfer, which indicate convergence, though some oscillations may nevertheless occur.

Table 2. Simulation runs – Influence of time step size

Sim. Index	Cooling	Sim. Type	Load Case	Time Step	Run Time (for 8 cores)
B13	Flooded cooling (water)	Transient (360 s)	SST turbulence, w. buoyancy, w. rotation (3000 rpm)	0.1 s (~0.5/rev)	106402 s (~1d 4h)
B12	Flooded cooling (water)	Transient (360 s)	SST turbulence, w. buoyancy, w. rotation (3000 rpm)	0.01 s (~2/rev)	1199923 s (~13d 21h)
B15	Flooded cooling (water)	Transient (360 s)	SST turbulence, w. buoyancy, w. rotation (3000 rpm)	0.005 s (~4/rev)	2335600 s (~27d 1h)
B14	Flooded cooling (water)	Transient (360 s)	SST turbulence, w. buoyancy, w. rotation (3000 rpm)	0.0025 s (~8/rev)	4748688 s (~54d 23h)

To ensure convergence and numerical reliability of the solution, several tool temperature monitoring points were checked. Figure 5 shows this for the stationary simulation B2.

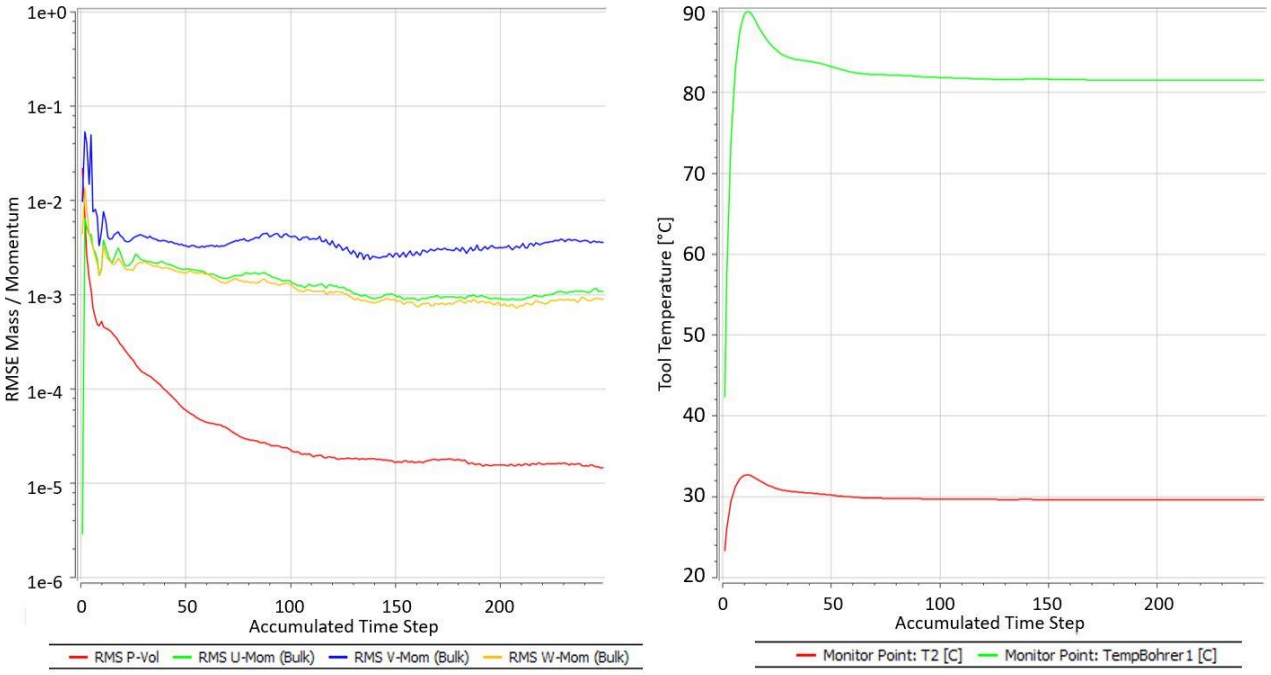

Fig. 5. Mass and momentum residuals (left) and tool temperatures (right) for simulation B2

3.2. INVESTIGATION OF THE INFLUENCE OF WATER COOLING

In the experimental investigation, a mix of 94% water and 6% lubricant was used for the tool cooling. First, to get a general sense of the effect of the coolant on the tool temperature, simulations with and without flooded water cooling were compared. Table 3 shows the resulting temperatures of the tool. Here, as well as in the following sections, the mean temperature refers only to the front, helical section of the tool. This comparison shows a significant cooling effect for the tool using flooded water cooling. The resulting temperature field is shown in Figure 6 (left). Figure 6 (right) shows the movement / flow and velocity of

the water particles for the simulated water cooling. The origin of the flow is the cooling nozzle shown in Figs. 1 and 2.

Table3. Simulation runs – Influence of water cooling

Sim. Index	Cooling	Sim. Type	Load Case	Max. Tool Temperature	Mean Tool Temperature
B1	No cooling	Steady state	laminar, w/o. buoyancy, w/o. rotation	100.6°C	60.6°C
B2	Flooded cooling (water)	Steady state	laminar, w/o. buoyancy, w/o. rotation	62.2°C	38.0°C

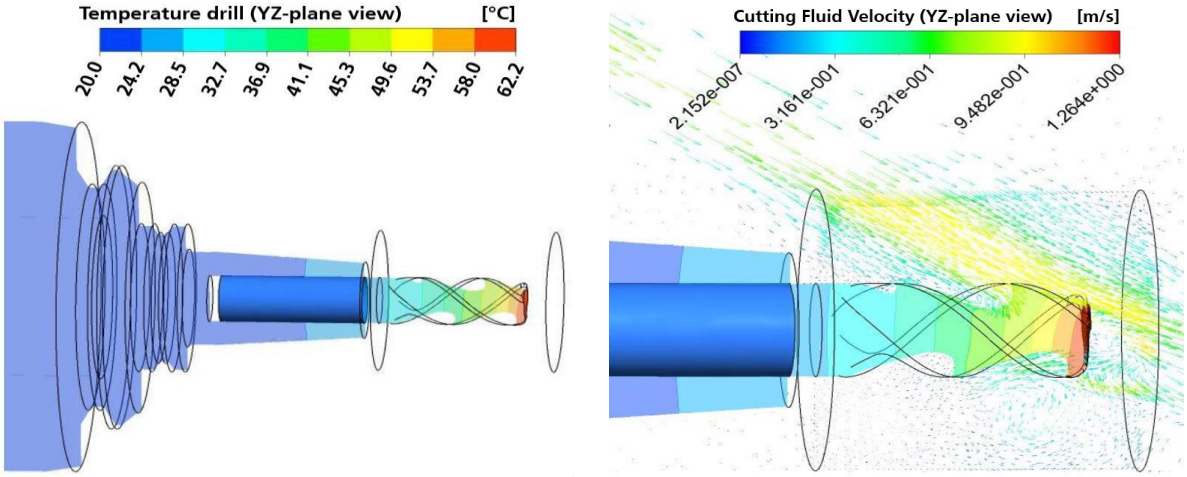

Fig. 6. Simulated temperature field and fluid velocity of tool with water cooling for steady state (B2)

3.3. COMPARISON OF DIFFERENT TURBULENCE MODELS

There are different turbulence models to describe the non-laminar movement of fluids. The following comparison reveals the different effects of laminar flow vs. *k*-ε-turbulence model vs. Menter's shear stress transport (SST) turbulence model. The k-ε-turbulence model produces good results for interior flows but works poorly near the fluid volume boundary (walls). Therefore, the *k*-ω-model was developed to better predict the effects fluid-wall-contacts. The SST-model combines both by using the standard *k*-ε-turbulence model and switching to the *k*-ω-model near the walls [19].

Table 4. Simulation runs – Influence of turbulence model type without buoyancy

Sim. Index	Cooling	Sim. Type	Load Case	Max. Tool Temperature	Mean Tool Temperature
B2	Flooded cooling (water)	Steady state	laminar, w/o. buoyancy, w/o. rotation	62.2°C	38.0°C
B3	Flooded cooling (water)	Steady state	*k*-ε-turbulence, w/o. buoyancy, w/o. rotation,	50.3°C	30.4°C
B4	Flooded cooling (water)	Steady state	SST turbulence, w/o. buoyancy, w/o. rotation,	44.3°C	27.2°C

Table 4 compares both model types to each other and to a laminar coolant flow using steady-state simulations. The results show a notable impact of turbulence on the cooling effect in general and a slightly greater cooling effect for the SST model compared to the *k*-ε-turbulence model. The computation time with the SST model is about twice that of the laminar case and around 25% higher than with the *k*-ε-model. The same comparison with the consideration of buoyancy (an upward force countering gravity due to pressure gradients) is shown in Table 5.

Table 5. Simulation runs – Influence of turbulence model type with buoyancy

Sim. Index	Cooling	Sim. Type	Load Case	Max. Tool Temperature	Mean Tool Temperature
B5	Flooded cooling (water)	Steady state	laminar, with buoyancy, w/o. rotation	82.4°C	47.8°C
B6	Flooded cooling (water)	Steady state	*k*-ε-turbulence, with buoyancy, w/o. rotation,	68.5°C	37.6°C
B7	Flooded cooling (water)	Steady state	SST turbulence, with buoyancy, w/o. rotation,	63.3°C	35.3°C

Once again, the cooling effect increases with the addition of turbulence, though the difference between the two turbulence models is now less noticeable. The overall cooling effect with buoyancy is, however, much smaller than without buoyancy. This is because the gravity shifts the flow of the cooling jet towards the center of the tool, away from the heat source. Figure 7 shows this effect, particularly when compared to Fig. 6.

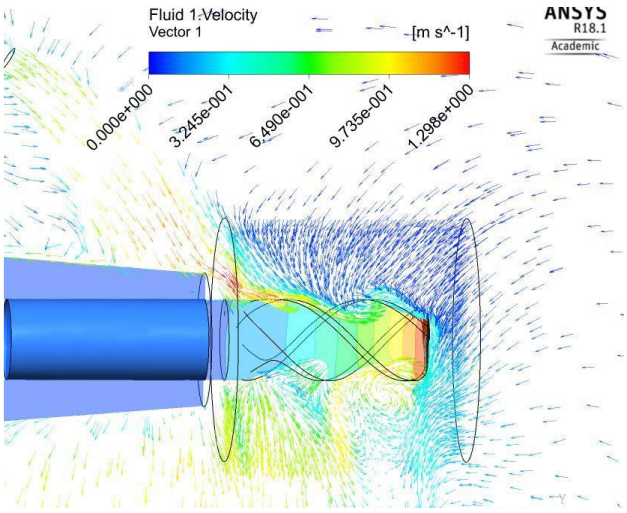

Fig. 7. Fluid flow velocity for flooded water cooling (B7, with buoyancy, turbulent)

Figure 8 shows the laminar case (B5) in a slightly altered flow velocity representation. In practice, the fluid stream bending would be remedied by changing the angle of the cooling nozzle or increasing the speed of the coolant flow. For a steady-state simulation, ignoring gravity is not sensible since it has little effect on computation time and may even deliver implausible results. For transient simulations with rotating fluid domains, where the gravity

vector changes constantly, eliminating gravity may be considered, depending on the scenario and the specific purpose of the investigation. Ignoring buoyancy may also be interesting in another scenario. If the machine tool has a kinematic configuration that can change the orientation of the tool relative to gravity, then it would be very helpful to only have to simulate the cooling behaviour for a single configuration, rather than for a larger set of discrete tool orientations. In any case, however, the results above suggest that this simplification may lead to unacceptably high errors. These errors may be much lower for very high-pressured fluid streams, where gravity play less of a role.

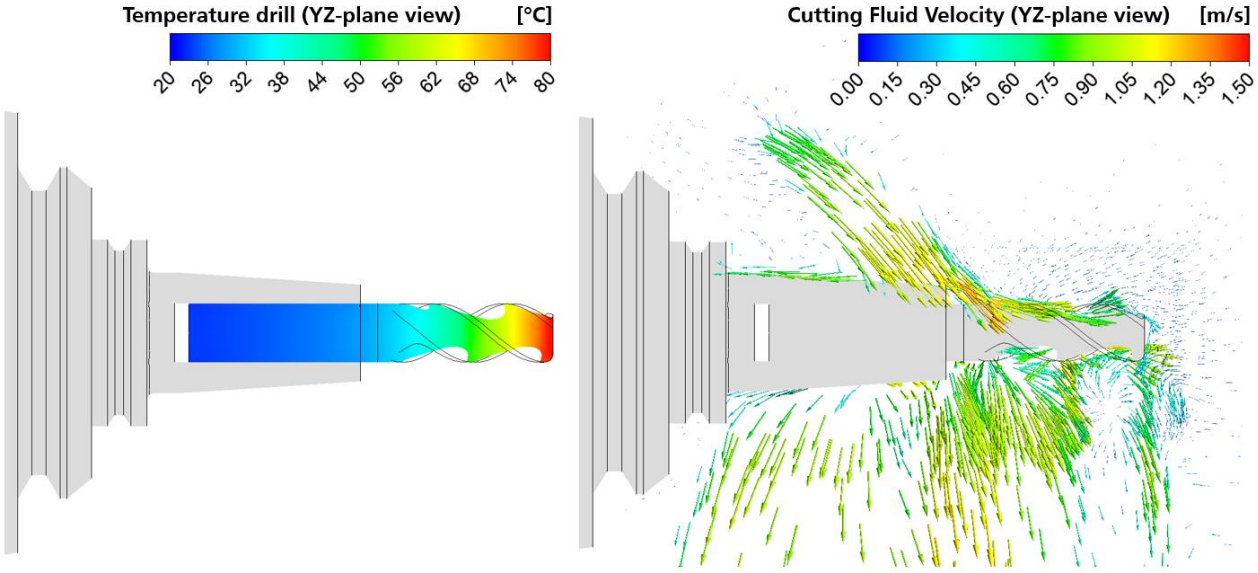

Fig. 8. Fluid flow velocity for flooded water cooling (B5, with buoyancy, laminar)

3.4. COMPARISON OF THE COOLING EFFECT OF DIFFERENT COOLANTS

Previously, to simplify the load case, it was decided to start with pure water as a coolant. Table 6 now compares the four basic load cases from chapter 2 and shows, what difference the addition of lubricant makes to the cooling effect and how air cooling compares to water cooling.

Table 6. Simulation runs – Influence of coolant type

Sim. Index	Cooling	Sim. Type	Load Case	Max. Tool Temperature	Mean Tool Temperature
B7	Flooded cooling (water) [LC1]	Steady state	SST turbulence, with buoyancy, w/o. rotation,	63.3°C	35.3°C
B8	Flooded cooling (water + lubricant) [LC2]	Steady state	SST turbulence, with buoyancy, w/o. rotation,	69.3°C	37.6°C
B9	Air cooling (air) [LC3]	Steady state	SST turbulence, with buoyancy, w/o. rotation,	100.3°C	60.6°C
B10	Oil-air cooling (air + lubricant) [LC4]	Steady state	SST turbulence, with buoyancy, w/o. rotation,	94.8°C	55.6°C

Table 6 shows that the lubricant reduces the cooling effect of water slightly. Compressed air, at the tested air speed, achieves almost no noticeable cooling effect. The flow speed would need to be increased significantly in order to improve tool cooling. The addition of lubricant to air improves the cooling effect of air, as might be expected, though it still remains low. For most relevant applications, lubricants are important for increasing tool life by reducing friction, plus they also decrease the waste heat from cutting.

3.5. STATIONARY VS. TRANSIENT CALCULATION

In order to evaluate, how steady-state simulations differ from transient simulations in scenarios without tool rotation, both simulation types are compared in Table 7 for water cooling.

Table 7. Simulation runs – Steady-state vs. transient simulation

Sim. Index	Cooling	Sim. Type	Load Case	Max. Tool Temperature	Mean Tool Temperature
B7	Flooded cooling (water) [LC1]	Steady state	SST turbulence, with buoyancy, w/o. rotation	63.3°C	35.3°C
B11	Flooded cooling (water) [LC1]	Transient (360 s)	SST turbulence, with buoyancy, w/o. rotation	63.3°C	35.1°C

Table 7 shows a good agreement between steady-state und transient simulations for the investigated load case. Figure 9 shows the flow velocity of the water coolant in the *y*-*z*-plane.

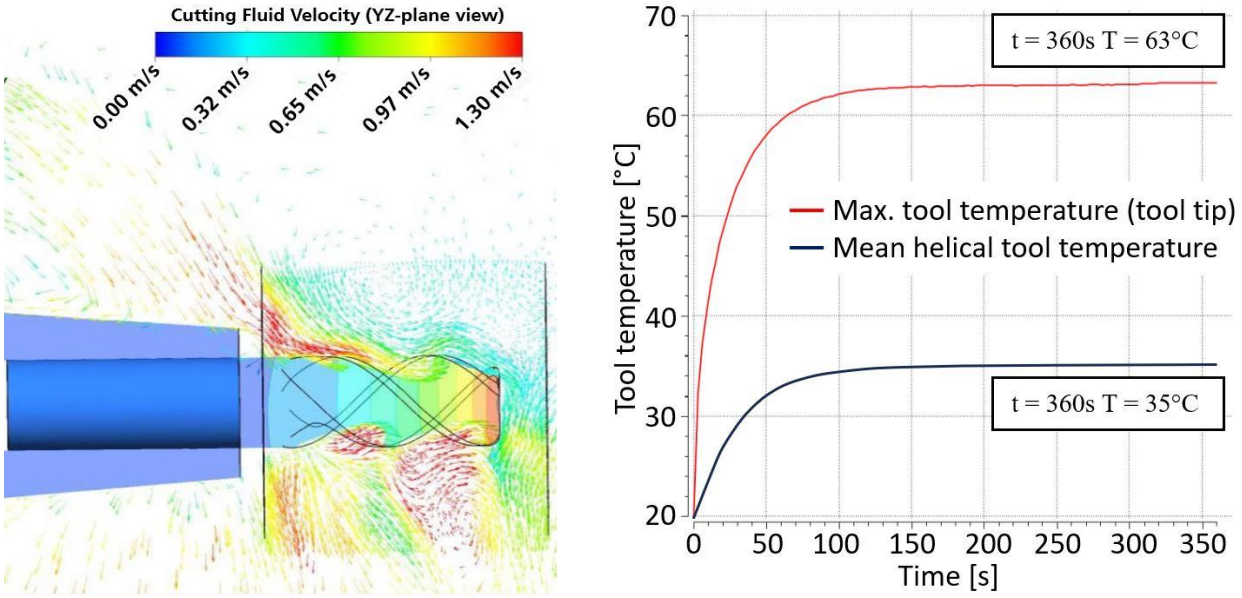

Fig. 9. Fluid flow velocity (left) and max/mean tool temperatures (right) for flooded water cooling (B11)

3.6. INVESTIGATION OF THE TOOL ROTATION ON THE HEAT TRANSFER FROM TOOL TO COOLANT

For the modelling of the tool rotation, a cylindrical hull was added as an additional fluid domain, see Fig. 2. Since the tool rotation causes the rotational axis to deviate from the gravitational axis, transient simulations are required instead of the previously used steady-state simulations. Buoyancy was also included here, since it was already established, that it has a significant effect on the coolant flow vectors and thus the cooling rate. Table 8 shows the effect that the rotation of tool and spindle has on the resulting temperature field inside the tool. A spindle speed of 3,000 rpm and a time step size of 0.01 s (~2 steps/rev) were selected. Once again, the stationary state was reached after about 100 s of simulated time, though there remained temperature fluctuations after this point, see Fig. 10.

Table 8. Simulation runs – Influence of tool rotation

Sim. Index	Cooling	Sim. Type	Load Case	Max. Tool Temperature	Mean Tool Temperature
B11	Flooded cooling (water) [LC1]	Transient (360 s)	SST turbulence, with buoyancy, without rotation	63.3°C	35.1°C
B12	Flooded cooling (water) [LC1]	Transient (360 s)	SST turbulence, with buoyancy, with rotation 3000 rpm	47.0°C	27.8°C

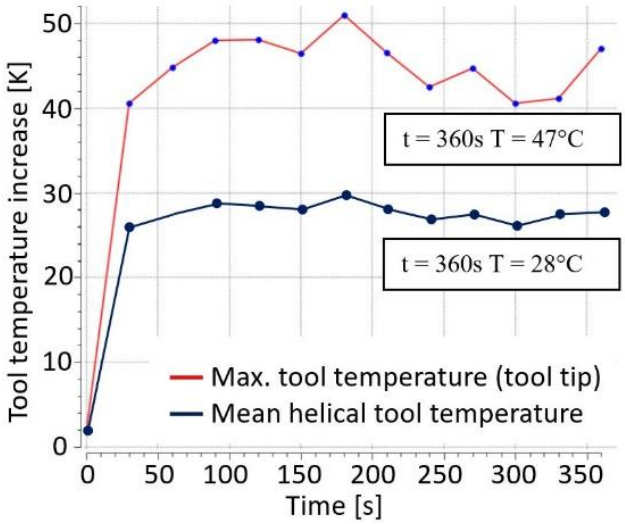

Fig. 10. Maximum and mean tool temperature increases for 360s transient simulation (B12)

The simulated additional cooling effect from modelling the tool and spindle rotation was around 20-25% (w.r.t. 20°C ambient temperature), which is quite significant. Like in the previous sections, Fig. 11 shows the corresponding fluid velocity vectors in the *y*-*z*-plane. The simulation shows how the fluid creates recirculation zones above and below the helical tool section, which increase the cooling effect. In order to better visualize and quantify the cooling effect, Fig. 12 shows the heat flux, where a strong negative flux signifies a high cooling rate. This occurs particularly at the front of the tool and along the outside, bladed part of the helical tool section.

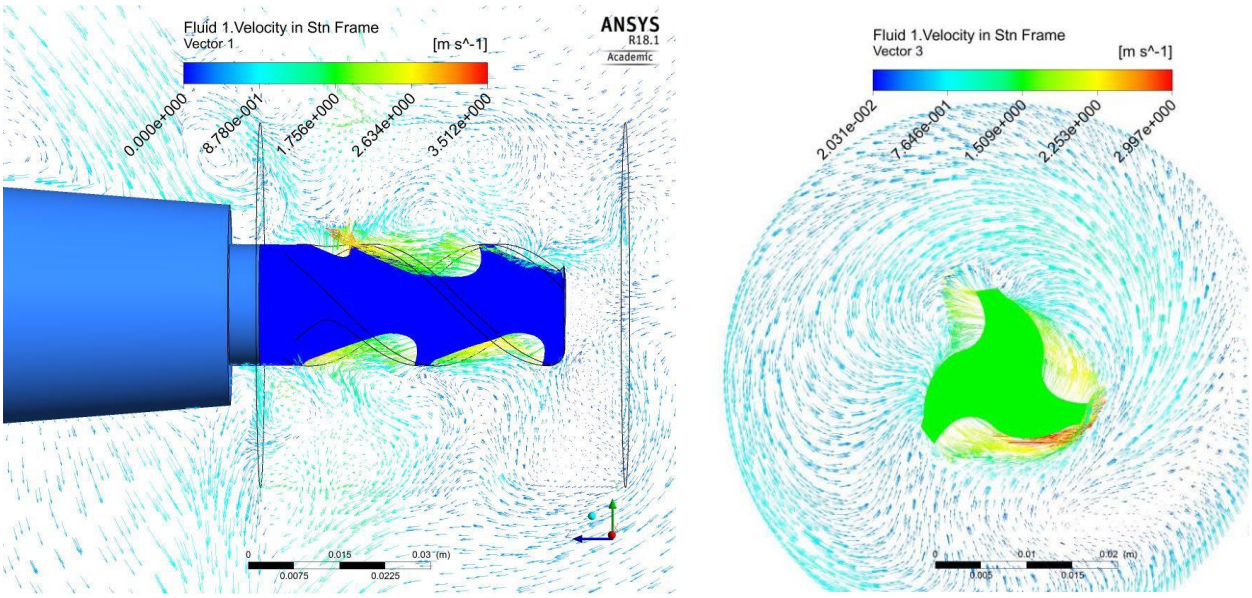

Fig. 11. Fluid flow velocity for flooded water cooling (B12); left: side view, right: front view (ccw. rotation)

As was noted before, the consideration of buoyancy causes the coolant jet to hit the rear section of the tool. Figure 11 shows how much of the cooling results from the coolant being sucked in and pulled along by the rotating tool. A significant portion of the coolant also has little or no contact with the heated tool sections and thus effectively only acts on the machining table and workspace.

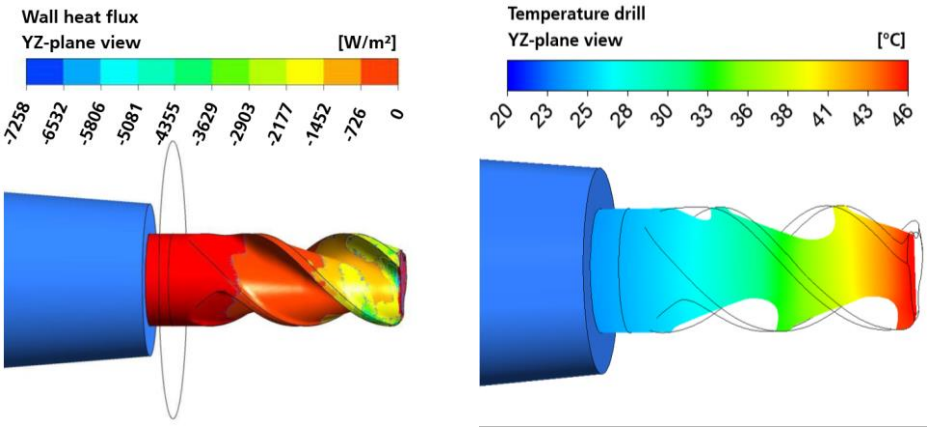

Fig. 12. Left: Heat flux for water cooling (B12), Right: corresponding temperature field

4. EXPERIMENTAL INVESTIGATION OF THE RELATION BETWEEN TOOL COOLING AND TOOL ROTATION

Alongside the modelling and simulation of the thermal tool behaviour under different cooling scenarios, several measurements were also conducted. The test stand, for which the simulation model was created, is shown in Fig. 13. It comprises the spindle, chuck, tool, coolant nozzle, four temperature sensors and the induction heater, which simulates the heat

from the cutting process. This setup allows the measurement of the temperature distribution in the tool with a defined heat source at low to high rotational speeds and with different cooling strategies (water, air, MQL).

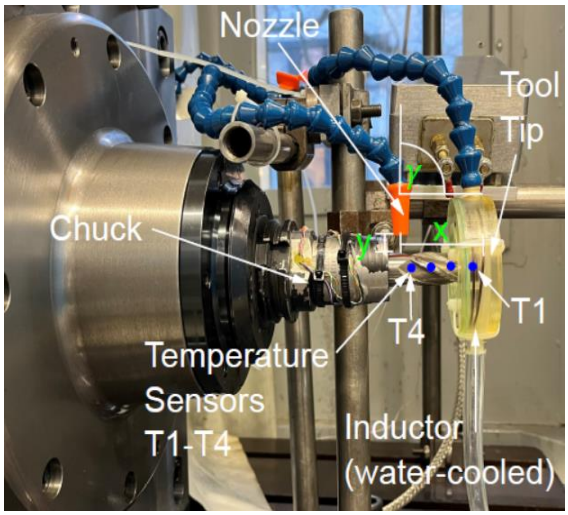

Fig. 13. Test stand for investigating the thermal behaviour of spindle and tool

The nozzle orientation in Fig. 13 does not match the experimental one since the image was taken at a later time. The four PT100 temperature sensors were placed at 10 mm (T1), 20 mm (T2), 35 mm (T3) and 55 mm (T4) distance from the front of the tool. The sensors are small contacting sensors placed inside the hollowed-out tool. The sensors have short cables which are connected to a slip ring, so that they can operate during tool rotation without twisting up the cables. In order to validate the simulations, a test with three different spindle rotation speeds was performed, see Fig. 14.

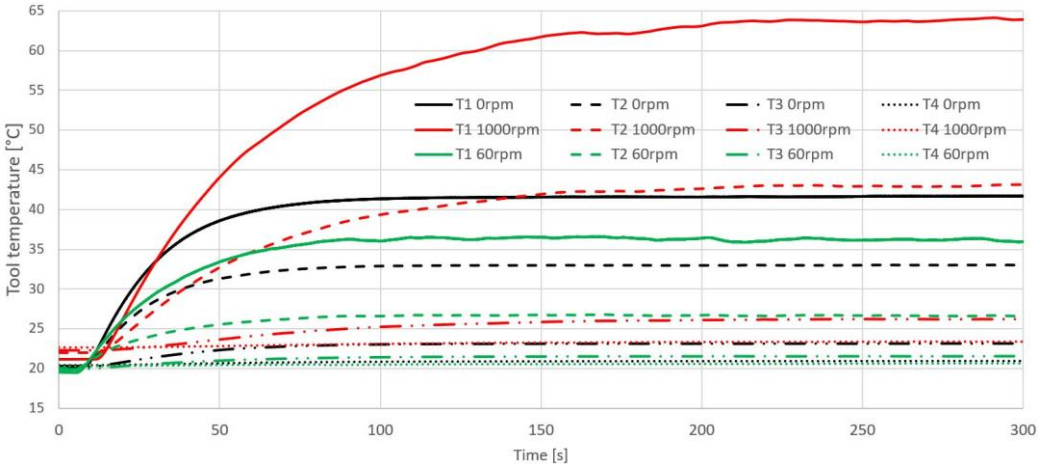

Fig. 14. Temperature distribution of the tool under flooded cooling with 0, 60 and 1000 rpm

Contrary to the results of simulations B11 and B12, the cooling rate for 60 rpm is noticeably larger than that for 0 rpm (+12%), but for the much higher 1000 rpm it is

significantly reduced (-52% compared to 0 rpm). This is likely because the tool, at high rotational speeds, reflects the coolant back into the workspace and thereby prevents the large surface of the helical section of the tool from properly contacting the coolant for any significant length of time. Cooling via forced convection from the tool rotation still occurs, but the flooded cooling barely affects the tool and acts mostly on the workpiece, machining table and workspace. Modelling this real observed cooling behaviour in the CFD simulations can be accomplished by reducing the size of the rotating fluidic domain (see Fig. 2).

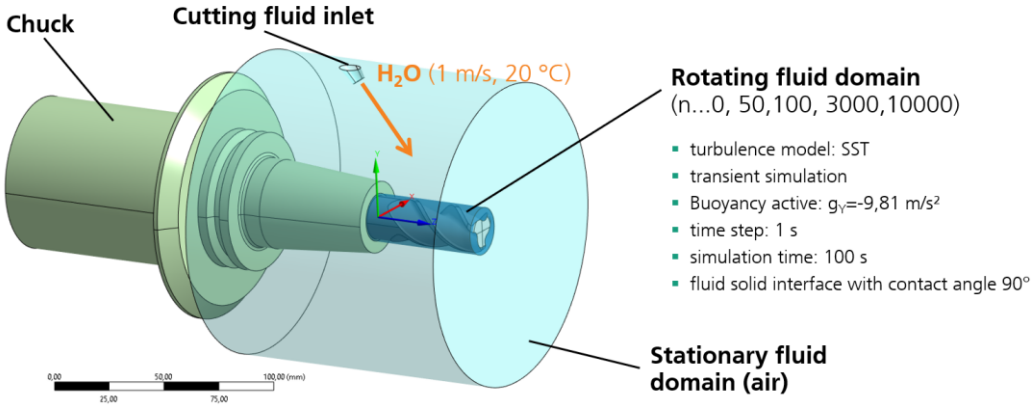

Fig. 15. Improved tool and workspace model for simulating cooling behaviour with tool rotation

The large hull, which was initially used, creates additional terms in the conservation equations, which leads to larger numerical errors. This results in unnatural fluid flows, which do not coincide with reality. By reducing the size of this domain as much as possible, the uncertainties in the model could be greatly reduced. Figure 15 shows the new model with boundary conditions.

A boundary layer mesh was used near the wall. This was also one of the improvements in contrast to the original simulation model with the larger rotating domain. An image was added to show this. The employed SST-turbulence model is suitable for both high and low *Re* values and any *Y*+ values up to 300. Figure 16 shows this boundary layer mesh on the left and in comparison, the previous mesh without boundary layers on the right. Figures 17 and 18 show the simulated flow of cutting fluid for different rotation speeds and Fig. 19 illustrates the reversal of the cooling behaviour between 1,000 and 3,000 rpm.

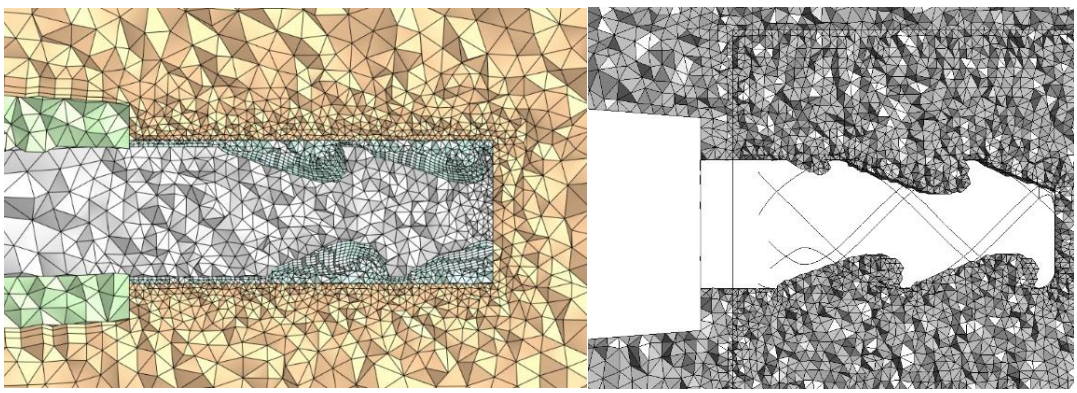

Fig. 16. Mesh around tool: (left) new mesh with boundary layers, (right) old mesh without

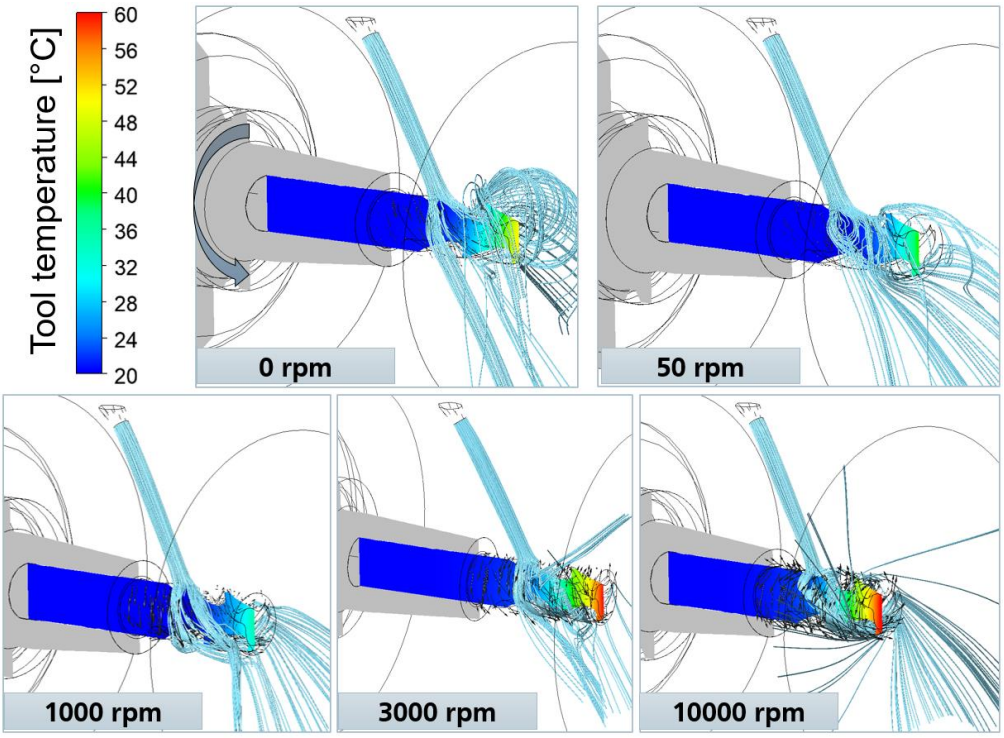

Fig. 17. Tool temperature and fluid flows for different rotation speeds

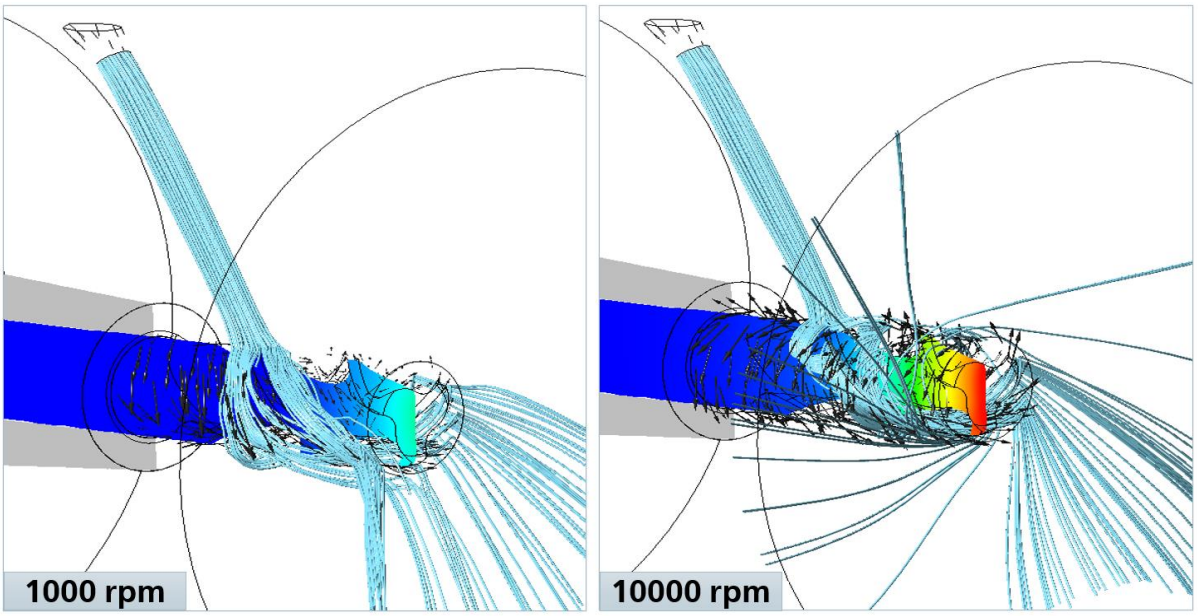

Fig. 18. Tool temperature and fluid flows for 1,000 vs 10,000 rpm

The exact rotation speed for optimal cooling will vary depending on the angle and speed of the cutting fluid from the inlet. This is most likely also the reason, why in the experiment, the cooling rate reversed before 1000 rpm and not until higher rpms. The cooling rate is visually apparent when comparing the tool temperatures (especially in the stationary state) under different experimental conditions (e.g. rpms). It can also be quantified using the heat

transfer coefficient, which is shown in Fig. 20 for 0 rpm, 1,000 rpm and 10,000 rpm after 100 s (final time step) as computed from the ANSYS CFD model. The grey cutting fluid mist in the image also gives an indication as to why certain sections of the tool have higher cooling rates.

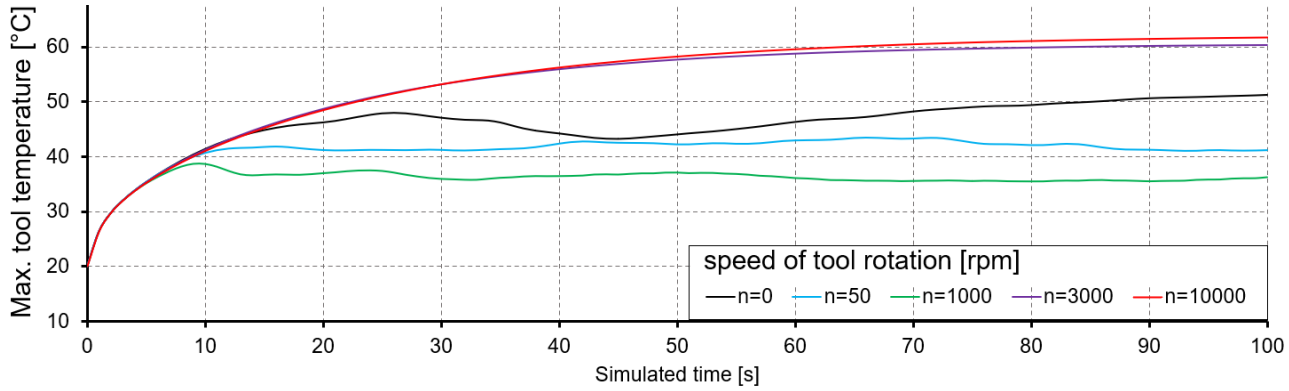

Fig. 19. Max. tool temperature with cutting fluid use at various rotational speeds

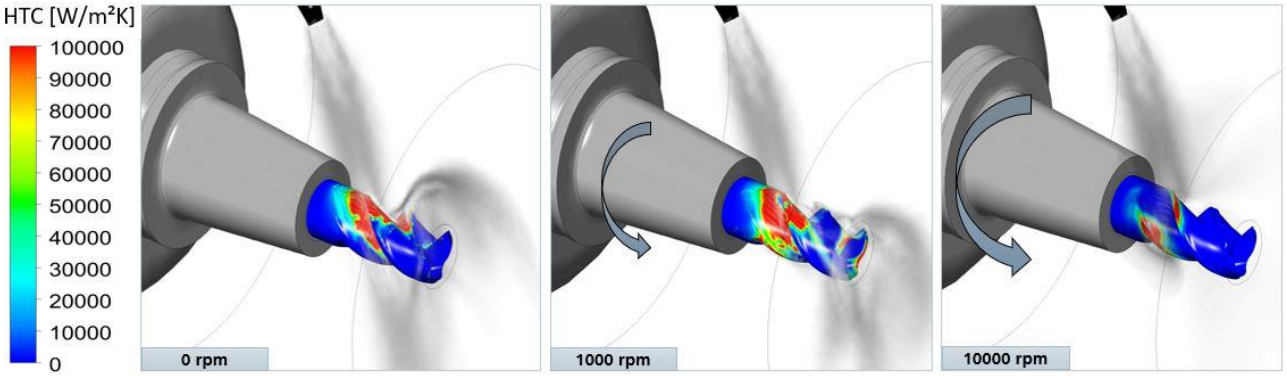

Fig. 20. Heat transfer coefficients (HTCs) with cutting fluid use at various rotational speeds for time 100 s

This comparison is not meant to suggest that rotation speeds should be chosen based on the cooling rate. Instead, overly large amounts of cutting fluid used at high rotation speeds should be questioned in terms of effectiveness vs. cost. Higher fluid velocities with narrow aimed streams (jet cooling) may also lead to better cooling at higher rotational speeds.

In terms of thermal error, it is also interesting to observe what elongation (Δz) and radial expansion ($\Delta \varnothing$) of the tool result from these various tool temperatures. Figure 21 shows that the tool deformation even with the use of cooling lubricant is significant. However, since the temperature gradient of the tool is large near the tool tip and falls quickly towards the tool holder (see Figs. 8 and 14), the absolute deformation values are not as large as the tool tip temperature might suggest. Still, false modelling of the cooling rate in the tool, especially with high process heat, may lead to an underestimation of the thermal error of up to 10 µm, just from the rather small cutting tool. While this deformation is normally easy to compensate using an offset, the situation becomes more difficult, when frequent tool changes are made.

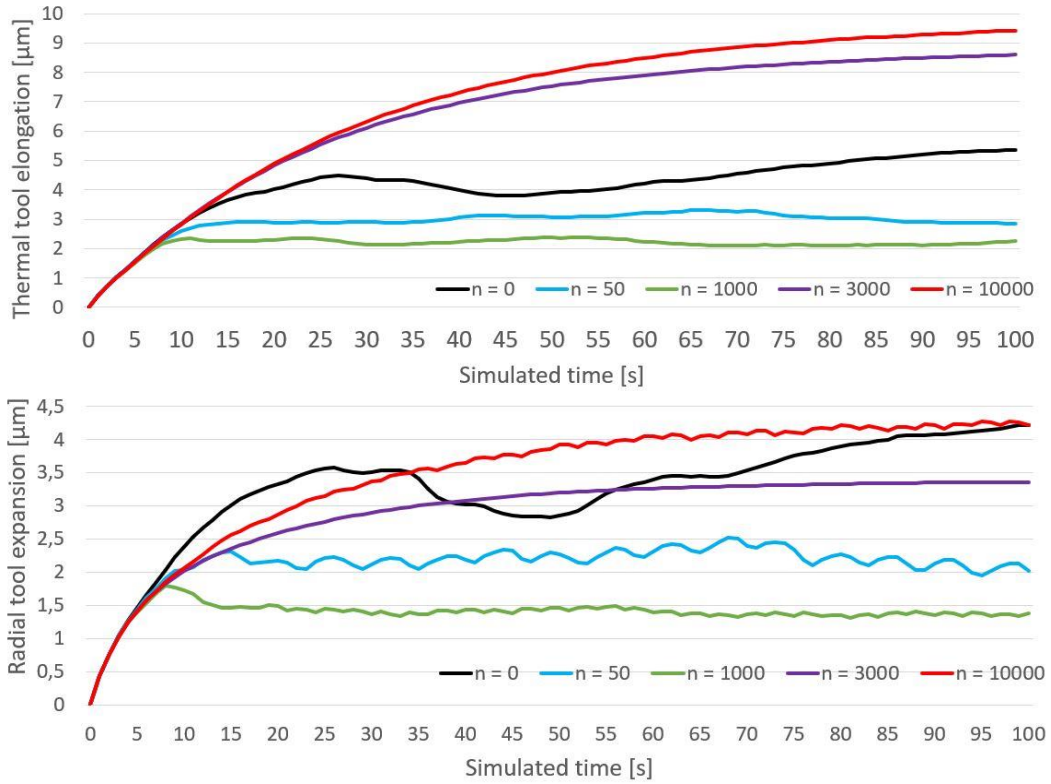

Fig. 21. Tool elongation and radial expansion (near the tool tip) with cutting fluid use at various rotational speeds

5. INFLUENCE OF CHIPS ON TOOL COOLING

Another important aspect, which has been mostly ignored in the above-described investigations, is the influence of chips on the tool cooling. Most thermal research on chips has been on the ratio in which the process heat is divided into chip, tool, workpiece and cutting fluid. It is, however, also interesting to investigate, to what degree chips might impede tool cooling. There are several challenges with including chips. From a practical point of view, the physical test stand (Figs. 1, 13) cannot be used for actual cutting operations due to the lack of a necessary kinematic axis. Performing cutting operations on a real machine tool is possible but makes it more difficult to determine the exact heat influx into the tool. There are also many different shapes of chips depending, among other aspects, on tool geometry, workpiece material and cutting parameters. Including chips into the transient CFD model is theoretically possible but very difficult, because CFD mainly uses the fluid finite volume model of the workspace and changing geometries in the solid model are normally not desired and would require a very fine dynamic mesh and coupled fluid-structure interactions. In addition, it would hardly be possible to resolve the heat transfer at the solid-fluid interface with a structured mesh, because the mesh generation leads to a negative Jacobi determinant if the gap for the fluid is too small. It may be possible with a tetrahedral mesh, but then a resource-efficient resolution of the processes near the wall can no longer be obtained. In terms of heat flow, this is already implicitly included in the current model. The contact zone between tool and workpiece/chip is not affected by the coolant (no cooling boundary condition).

Quantitatively, very little cutting fluid will actually be impeded by the chips, especially when using flooded cooling at high rpms, where no large chip nests are formed near the tool. For the straight shank drill bit used here, the chip could wind itself upwards along the tool channels and thus cover a larger part of the tool geometry. This case may be interesting, particularly how this affects the cooling rate at various tool rotation speeds. This aspect will be one part in a new, upcoming research project.

6. SUMMARY AND OUTLOOK

Thermal errors in machine tools still present a major challenge in maintaining positioning accuracy during cutting operations. Next to the thermal deformation of the machine tool, the expansion of the cutting tool and other operational effects within the machining workspace can also have a large influence on the accuracy of the manufactured workpieces.

The paper describes a test stand for the investigation of the cooling effects using different methods of tool cooling and also on how they can be simulated using CFD and FEM simulations. For this, a simulation model and the applied boundary conditions were explained. Simulation runs with different settings were used to explore optimal or poor simulation settings, and computation times and numerical errors were investigated.

Transient simulations with turbulence, buoyancy and tool rotation (3,000 rpm) showed large temperature fluctuations of over 10K in the quasi-stationary state, which could be reduced with smaller time step sizes at the cost of extremely high computation times.

Using turbulence models in the simulations improved the cooling rate compared to laminar coolant flow, where the more exact SST turbulence model showed a stronger cooling rate than the simpler k-ε-model. This added precision comes at the cost of longer computation time for the SST turbulence model.

A comparison of different coolant types showed that pure water worked best, while the addition of 6% lubricant increased the tool temperature by only a few Kelvin. Pure air (at the investigated pressure) had almost no effect. Adding a small amount of lubricant to the air showed a small improvement of the cooling by about 10%. Neglecting buoyancy in the simulation showed a large impact on the computed cooling effect, though this was mixed with a change in the vector and position at which the cutting fluid struck the tool.

Simulations with tool rotation required transient calculations due to the changing gravity vector relative to the rotating fluid domain. For simulations without tool rotation, however, transient and stationary simulations showed nearly identical results.

Simulations with tool rotation (3,000 rpm) and water cooling initially showed a strong cooling effect, which was about 40–50% stronger than without rotation. Measurements performed at the physical test stand, however, showed the opposite behaviour. There, the cooling rate initially increased for low rotational speeds and then decreased for higher speeds. Using an improved simulation model with a very narrow rotating fluid domain, this reversal of the cooling effect could be reproduced. The new model showed, how at high rotation speeds, the fluid is reflected from the tool and does not properly contact the tool surface.

Finally, thermo-elastic simulations for water cooling, showed that the heating of the tool led to thermal tool elongation of up to 9 μm and radial tool expansion of up to 4 μm.

Subsequent research will be directed towards the implementation of reliable real-time tool deformation prediction. This will be linked with a process simulation to obtain the process heat input and machine control data for spindle speeds and cooling system parameters. In addition, the effects of the coolant on the workspace will be investigated and how adiabatic (evaporative) cooling affects the walls of the machine tool workspace. Finally, an investigation of the effects of chips on tool cooling is planned.

ACKNOWLEDGEMENTS

This research was funded by the German Research Foundation (DFG) as part of the project - Modelling of dual-phase fluid-solid interactions in the workspace of cutting machine tools to enable process-specific thermal error compensation (ID 174223256), which is hereby gratefully acknowledged.

REFERENCES

[1] BRÄUNIG M., REGEL J., RICHTER C., PUTZ M., 2018, *Industrial Relevance and Causes of Thermal Issues in Machine Tools, In Conference Proceedings*, 1st Conference on Thermal Issues in Machine Tools, Dresden.

[2] BRINKSMEIER E., MEYER D., HUESMANN-CORDES A.G., HERRMANN C., 2015, *Metalworking Fluids - Mechanisms and Performance*, CIRP Annals – Manuf. Techn. 64/2, 605–628, https://doi.org/10.1016/j.cirp.2015.05.003.

[3] KIZAKI T., TSUJIMURA S., MARUKAWA Y., MORIMOTO S., KOBAYASHI H., 2021, *Robust and Accurate Prediction of Thermal Error of Machining Centers Under Operations with Cutting Fluid Supply*, CIRP Annals 70/1, 325–328, https://doi.org/10.1016/j.cirp.2021.04.074.

[4] MAYR J., GEBHARDT M., MASSOW B., WEIKERT S., WEGENER K., 2014, *Cutting Fluid Influence on Thermal Behavior of 5-Axis Machine Tools*, Procedia CIRP 14, 395–400, https://doi.org/10.1016/j.procir.2014.03.085.

[5] PAVLIČEK F., BEER Y., WEIKERT S., MAYR J., WEGENER K., 2016, *Design of a Measurement Setup and First Experiments on the Influence of CO_2-Cooling on the Thermal Displacements on a Machine Tool*, Procedia CIRP 46, 23–26, https://doi.org/10.1016/j.procir.2016.04.075.

[6] HERNANDEZ-BECERRO P., BLASER P., MAYR J., WEIKERT S., WEGENER K., 2017, *Measurement of the Effect of the Cutting Fluid on The Thermal Response of a Five-Axis Machine Tool*, Lamdamap XII, euspen, London, 1–7.

[7] PERRI G.M., BRÄUNIG M., GIRONIMO D., PUTZ M., TARALLO A., WITTSTOCK V., 2016, *Numerical Modelling and Analysis of The Influence of an Air Cooling System on a Milling Machine in Virtual Environment*, Int. J. Adv. Manuf. Technol., 86, 1853–1864, https://doi.org/10.1007/s00170-015-8322-5.

[8] PUTZ M., WITTSTOCK V., SEMMLER U., BRÄUNIG M., 2016, *Simulation-Based Thermal Investigation of the Cutting Tool in the Environment of Single-Phase Fluxes*, Int. J. Adv. Manuf. Technol. 83, 117–122, https://doi.org/10.1007/s00170-015-7488-1.

[9] MICHALEK D.J., HII W.W-S., SUN J., GUNTER K.L., SUTHERLAND J.W., 2003, *Experimental and Analytical Efforts to Characterize Cutting Fluid Mist Formation and Behavior in Machining*, Appl. Occup. Environ. Hyg. 18/11, 842–854, https://doi.org/10.1080/10473220390237368.

[10] DANIEL C.M., RAO K.V.C., OLSON W.W., SUTHERLAND J., 1996, *Effect of Cutting Fluid Properties and Application Variables on Heat Transfer in Turning and Boring Operations*, Japan/USA Symposium on Flexible Automation 2, 1119–1126.

[11] LÓPEZ DE LACALLE L.N., ANGULO C., LAMIKIZ A., SÁNCHEZ J.A., 2006, *Experimental and Numerical Investigation of The Effect of Spray Cutting Fluids in High Speed Milling*, J. Mater. Process. Technol. 172/1, 11–15, https://doi.org/10.1016/j.jmatprotec.2005.08.014.

[12] BRECHER C., BÄUMLER S., JASPER D., TRIEBS J., 2012, *Energy Efficient Cooling Systems for Machine Tools*, Dornfeld, Linke (Eds.) Leveraging Technology for a Sustainable World, Springer, https://doi.org/10.1007/978-3-642-29069-5_41.
[13] BRÄUNIG M., REGEL J., GLÄNZEL J., PUTZ M., 2018, *Effects of Cooling Lubricant on the Thermal Regime in The Working Space of Machine Tools*, Procedia Manufacturing 33, 327–334, https://doi.org/10.1016/j.promfg. 2019.04.040.
[14] DEHN M., PLUM F., BERTAGGIA N., NEUS S., ZONTAR D., BRECHER C., 2023, *Modeling the Thermal Machine Tool Error During Cooling Lubricant Usage*, Procedia CIRP 120, 1179–1184, https://doi.org/10.1016/ j.procir. 2023.09.145.
[15] JEDRZEJEWSKI J., WINIARSKI Z., KWASNY W., 2020, *Research on Forced Cooling of Machine Tools and its Operational Effects*, Journal of Machine Engineering 20/2, 18–38, https://doi.org/10.36897/jme/122769.
[16] TANABE I., SUZUKI N., ISHINO Y., ISOBE H., 2024, *Development of FEM Thermal Simulation Technology for Machine Tools with Enclosures and its Application*, Journal of Machine Engineering 24/1, 17–28, https://doi.org/ 10.36897/ jme/176716.
[17] MARES M., HOREJS O., FIALA S., HAVLIK L., STRITESKY P., 2020, *Effects of Cooling Systems on the Thermal Behaviour of Machine Tools and Thermal Error Models*, Journal of Machine Engineering 20/4, 5–27, https://doi.org/10.36897/jme/128144.
[18] GLÄNZEL J., NAUMANN A., KUMAR T.S., 2020, *Parallel Computing in Automation of Decoupled Fluid-Thermostructural Simulation Approach*, Journal of Machine Engineering 20/2, 39–52, https://doi.org/10.36897/ jme/117785.
[19] VERSTEEG H K., MALALASEKERA W., 2007, *An Introduction to Computational Fluid Dynamics – The Finite Volume Method*, 2nd Edition, Pearson, ISBN: 978-0-13-127498-3.